Dynamics of Formation and Fine Structure of Flow Pattern Around Obstacles in Laboratory and Computational Experiment

Yu. D. Chashechkin[1(✉)], Ya. V. Zagumennyi[2], and N.F. Dimitrieva[2]

[1] A.Yu. Ishlinskiy Institute for Problems in Mechanics of the RAS, Moscow, Russia
yulidch@gmail.com
[2] Institute of Hydromechanics of NAS of Ukraine, Kiev, Ukraine
zagumennyi@gmail.com, dimitrieva@list.ru

Abstract. Non-stationary dynamics and structure of stratified and homogeneous fluid flows around a plate and a wedge were studied on basis of the fundamental equations set using methods of laboratory and numerical modeling. Fields of various physical variables and their gradients were visualized in a wide range of the problem parameters. Eigen temporal and spatial scales of large (vortices, internal waves, wake) and fine flow components were defined. The same system of equations and numerical algorithm were used for the whole range of the parameters under consideration. The computation results are in a good agreement with the data of laboratory experiments.

Keywords: Fundamental system · Laboratory experiment · High-resolution computations · Flow around obstacles

1 Introduction

Since the pioneering papers by d'Alembert [1, 2] and Euler [3, 4] calculations of flow patterns around obstacles with evaluation of forces, acting on their surfaces, occupy a leading position in the theoretical and experimental fluid mechanics. Stability of the interest to the problem is supported by its fundamental content and complexity, as well as by diversity and importance of its practical applications. A particular attention is paid to calculation of flow around obstacles with a rather simple shape, e.g. plate, cylinder, sphere, etc., which symmetry is used for simplification of the governing equations [5].

Due to the complexity of analysis of the problem the traditional system of continuity and Navier-Stokes equations in the homogeneous fluid approximation is replaced by various model systems, among which the boundary layer and turbulence theories are the most widely used. However, new systems are characterized by their own symmetries not coinciding with these of the initial system of equations derived on basis of the general physical principles [6]. Accordingly, the physical meaning of the quantities denoted by the same symbols and the nature of their relations are changed in new sets. Such transformations make it difficult to verify experimentally the results and compare different mathematical models to each other.

V. Voevodin and S. Sobolev (Eds.): RuSCDays 2016, CCIS 687, pp. 41–56, 2016.
DOI: 10.1007/978-3-319-55669-7_4

The techniques of experimental and theoretical studies of fluid flows conducted at the Laboratory of Fluid Mechanics IPMech RAS are based on the fundamental system including equations of state and transport of substance, momentum and energy for inhomogeneous fluids [5].

In the environment, i.e. the Earth's hydrosphere and atmosphere, and industrial devices, fluid density, as a rule, is not constant due to inhomogeneity of either soluble substances or suspended particles concentration or temperature and pressure distributions. Under the action of buoyancy forces fluid particles with different density move vertically and form a stable continuous stratification which is characterized by buoyancy scale, $\Lambda = |d \ln \rho/dz|^{-1}$, frequency, $N = \sqrt{g/\Lambda}$, and period, $T_b = 2\pi/N$, which are supposed to be constant in space and can vary from a several seconds in laboratory conditions and up to ten minutes in the Earth's atmosphere and hydrosphere [7].

In the present paper we study numerically and experimentally flow patterns of a continuously stratified water solution of the common salt *NaCl* around 2D obstacles with aspect ratio of about 20. Two kinds of obstacles were examined including rectangular plates with different sizes and a wedge, which have been objects of thorough studies for the last century [8–10]. Main attention was paid to study the flow formation and visualization of a spatial structure of different physical variables field in a wide range of the flow condition.

2 Governing Equations, Basic Scales and Simulation Conditions

Mathematical modeling of the problem is based on the fundamental system of equation for multicomponent inhomogeneous incompressible fluid in the Boussinesq approximation [5] taking into account the buoyancy and diffusion effects of stratified components. In the study of slow, as compared to the speed of sound, flows of fluids characterized by high thermal conductivity, one can account in calculations only for variations in density associated with concentration of the stratified component neglecting temperature variations. Thus, the governing equations take the following form [8, 10]

$$\rho = \rho_{00}(\exp(-z/\Lambda) + s), \operatorname{div} \mathbf{v} = 0,$$
$$\frac{\partial \mathbf{v}}{\partial t} + (\mathbf{v}\nabla)\mathbf{v} = -\frac{1}{\rho_{00}}\nabla P + \nu\Delta\mathbf{v} - s \cdot \mathbf{g}, \quad \frac{\partial s}{\partial t} + \mathbf{v} \cdot \nabla s = \kappa_S \Delta s + \frac{\mathrm{v}_z}{\Lambda}. \tag{1}$$

Here, s is the salinity perturbation including the salt compression ratio, $\mathbf{v} = (\mathrm{v}_x, \mathrm{v}_y, \mathrm{v}_z)$ is the vector of the induced velocity, P is the pressure except for the hydrostatic one, $\nu = 10^{-2}$ cm^2/s and $\kappa_S = 1.41 \cdot 10^{-5}$ cm^2/s are the kinematic viscosity and salt diffusion coefficients, t is time, ∇ and Δ are the Hamilton and Laplace operators respectively.

The proven solvability of the two-dimensional fluid mechanics equations enables calculating flows around obstacles for both strongly ($\Lambda = 9.8$ m, $N = 1$ s^{-1}, $T_b = 6.28$ s) and weakly ($\Lambda = 24$ km, $N = 0.02$ s^{-1}, $T_b = 5.2$ min) *stratified* fluids,

and, as well, *potentially* ($\Lambda = 10^8$ km, $N = 10^{-5}\,\mathrm{s}^{-1}$, $T_b = 7.3$ days) and *actually homogeneous* media ($\Lambda = \infty$, $N = 0\ \mathrm{s}^{-1}$, $T_b = \infty$). In the case of *potentially* homogeneous fluid, density variations are so small that cannot be registered by existing technical instruments but the original mathematical formulation (1) is retained. In the case of *actually* homogeneous fluid, the fundamental system of equations is degenerated on the singular components [7].

The experiments and calculations were carried out in two stages. Initially, an obstacle with impermeable boundaries is submerged with minimum disturbances into a quiescent stratified environment. Physically reasonable initial and boundary conditions in the associated coordinate system are no-slip and no-flux on the surface of the obstacle for velocity components and total salinity respectively, and vanishing of all perturbations at infinity.

Diffusion-induced flow is formed due to interruption of the molecular transport of the stratifying agent on the obstacle [8]. The calculated flow is then taken as initial condition of the problem

$$\begin{array}{llll} \mathbf{v}|_{t\le 0} = \mathbf{v}_1(x,z), & s|_{t\le 0} = s_1(x,z), & P|_{t\le 0} = P_1(x,z), & \mathrm{v}_x|_\Sigma = \mathrm{v}_z|_\Sigma = 0, \\ \left[\frac{\partial s}{\partial \mathbf{n}}\right]\Big|_\Sigma = \frac{1}{\Lambda}\frac{\partial z}{\partial \mathbf{n}}, & \mathrm{v}_x|_{x,z\to\infty} = U, & \mathrm{v}_z|_{x,z\to\infty} = 0, & \end{array} \tag{2}$$

where, U is the uniform free stream velocity at infinity, $\mathbf{n}$ is external normal unit vector to the surface, Σ, of an obstacle which can be either a plate or a wedge with length, L, and height, h, or, $2h$.

The system of equations and the boundary conditions (1)–(2) are characterized by a number of parameters, which contain length $(\Lambda,\ L,\ h)$ or time $\left(T_b,\ \ T_U^L = L/U\right)$ scales and parameters of the body motion or dissipative coefficients.

Large dynamic scales, which are internal wave length, $\lambda = UT_b$, and viscous wave scale, $\Lambda_v = \sqrt[3]{g\nu}/N = \sqrt[3]{\Lambda\left(\delta_N^\nu\right)^2}$, characterize the attached internal wave fields structure [8, 10].

The flow fine structure is characterized by universal microscales, $\delta_N^\nu = \sqrt{\nu/N}$, $\delta_N^{\kappa_S} = \sqrt{\kappa_S/N}$, defined by the dissipative coefficients and buoyancy frequency, which are analogues of the Stokes scale on an oscillating surface, $\delta_\omega^\nu = \sqrt{\nu/\omega}$ [5]. Another couple of parameters such as Prandtl's and Peclet's scales are determined by the dissipative coefficients and velocity of the body motion, $\delta_U^\nu = \nu/U$ and $\delta_U^{\kappa_S} = \kappa_S/U$ [7, 8].

Relations of the basic length scales produce dimensionless parameters such as Reynolds, $\mathrm{Re} = L/\delta_U^\nu = UL/\nu$, internal Froude, $\mathrm{Fr} = \lambda/2\pi L = U/NL$, Péclet, $\mathrm{Pe} = L/\delta_U^{\kappa_S} = UL/\kappa_S$, sharpness factor, $\xi_p = L/h$ or fullness of form, $\xi_S = S/Lh$, where S is the cross-sectional area of an obstacle, and, as well, specific relations for a stratified medium. The additional dimensionless parameters includes length scales ratio, $C = \Lambda/L$, which is an analogue of the reverse Atwood number $\mathrm{At}^{-1} = (\rho_1 + \rho_2)/(\rho_1 - \rho_2)$ for a continuously stratified fluid.

Such a variety of length scales with their significant differences in values indicates complexity of internal structure even of such a slow flow generated by small buoyancy forces, which arise due to the spatial non-uniformity of molecular flux of the stratifying agent.

The large length scales prescribe size selection for observation or calculation domains, which should contain all the structural components studied, such as upstream perturbations, downstream wake, internal waves, vortices, while the microscales determine grid resolution and time step. At low velocities of the body motion, the Stokes scale is a critical one, while at high velocities the Prandtl's scale is dominant.

3 Laboratory Modeling of Flows Around a Plate

Experiments were carried out on the stands "Laboratory mobile pool" (LPB) and "Experimental stand for modeling of surface manifestations of underwater processes" (ESP) which belong to the Unique research facility "Hydrophysical complex for modeling of hydrodynamic processes in the environment and their impact on the underwater technical facilities, as well as the contaminant transfer in the ocean and atmosphere (URF "HPhC IPMech RAS")" [11]. The stands include transparent tanks with windows made of optical glass which allows using high-resolution optical observation devices such as the schlieren instruments IAB-451 and IAB-458. Models were fixed on transparent knives to the towing carriage, which moved along the guide rails mounted above the tank. Optical control of buoyancy profile and conductivity probe measurement of buoyancy frequency were carried out before starting the experiment. The following experiment was conducted after decay of all perturbations, which were registered by contact and optical instruments.

Scale of the phenomena under study was limited to the size of the viewing area of the schlieren instrument, which had diameter of 23 cm in these experiments. The spatial resolution, limited by the optical characteristics of the instrument itself and the recording equipment, which is being improved constantly with the development of computer technology, did not exceed 0.05 cm in these experiments. The classical "Vertical narrow slit-Foucault knife" and "Vertical slit-thread" techniques were used for flow visualization. In these methods, colour and brightness variations of a flow image are defined by value of the horizontal component of refraction index gradient [10, 11]. Refraction index of the sodium chloride water solutions is proportional to density, so schlieren images present patterns of the horizontal component of fluid density gradient.

Technical capabilities of the LPB and ESP stands enable visualizing both the main large-scale components of flows around obstacles, including upstream perturbations, downstream wakes, vortices, internal waves, and the fine structure elements such as high-gradient interfaces and filament in the both strongly and weakly stratified fluids.

Contours of phase surfaces of the upstream perturbations and attached internal waves in Fig. 1 are quite adequately described by the existing analytical and numerical models, which take into account geometry and velocity of body movement [8, 10].

Geometry of the high gradient interfaces, forming the environment fine structure, is very diverse and depends on the shape and velocity of the body movement and the stratification parameters, as well.

At small velocities of the body movement, sharp interfaces outline the density wake. These envelopes did not contact with the body at the poles but touch it inside the rear part (Fig. 1a). With increase in the plate velocity, the envelopes break down into

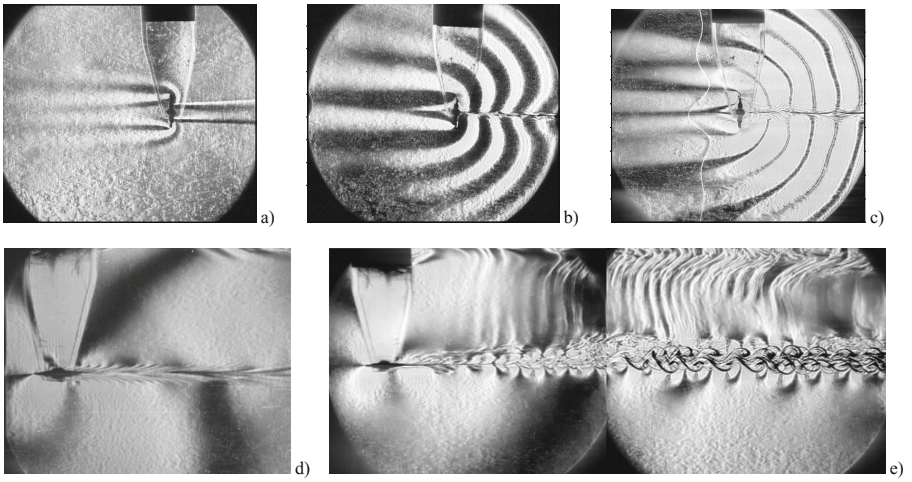

Fig. 1. Schlieren images of the flow pattern around a plate: (a–c) – placed vertically, $U = 0.03;\ 0.18;\ 0.29$ cm/s ($h = 2.5$ cm, $T_b = 12.5$ s); (d, e) – placed horizontally $U = 2.3;\ 4.9$ cm/s ($L = 2.5$ cm, $T_b = 7.5$ s).

filaments coexisting with internal waves in the central part of the downstream wake (Fig. 1b). With a further increase in velocity of the body movement shapes of the filaments are changed becoming similar to the forms of the phase surfaces of internal waves over a wide barrier, which generates waves with large amplitudes (Fig. 1c).

Another type of the fine structure was observed in the wake past a thin horizontal plate. Short filaments, forming a transverse structure (Fig. 1d), are well expressed here. With increase in velocity of the plate movement the filaments are lengthened and fill each compact vortex of the downstream wake, which is covered with its own high gradient envelope. With a further increase in the velocity the whole flow pattern takes a vortex structure (Fig. 1e) requiring for its resolution more precise instruments and high speed sensors.

4 Method for Numerical Simulation of Flow Around Obstacles

Numerical solution of the system (1) with the boundary conditions (2) was constructed using our own solver *stratifiedFoam* developed within the frame of the open source computational package OpenFOAM based on the finite volume method. The package, which was originally developed for numerical calculation of 3D problems in fluid mechanics, can effectively simulate 2D problems, as well, that is technically done by selection of only a single computational cell in the third dimension and specification of 'empty' boundary conditions on the front and back boundaries of the calculation domain.

In order to account for the stratification and diffusion effects, the standard *icoFoam* solver for unsteady Navier–Stokes equations in homogeneous viscous fluid was supplemented with new variables, including density ρ and salinity perturbation s, and corresponding equations for their calculation. We also added new auxiliary parameters such as buoyancy frequency and scale, N, Λ, diffusion coefficient, κ_S, acceleration due to gravity, g, and others. The Navier–Stokes equation for vertical velocity component and the diffusion equation were supplemented with the terms characterizing effects of buoyancy force and background stratification [12].

To interpolate the convective terms a limited TVD-scheme was used, which ensures minimal numerical diffusion and absence of solution oscillations. For discretization of the time derivative a second-order implicit asymmetric three-point scheme with backward differencing was used, which ensures a good time resolution of the physical process. For calculating the diffusion terms, based on the Gauss theorem within orthogonal grid sections, a surface normal gradient was evaluated at a cell face using a second order normal-to-face interpolation of the vector connecting centers of two neighboring cells. In non-orthogonal grid regions, an iterative procedure with a user specified number of cycles was used for non-orthogonal error correction due to a grid skewness.

Meshing of the computational domain was performed using the open integrable platform SALOME, which allows creating, editing, importing, and exporting CAD (Computer Aided Design) models, as well as building a grid for them, using different algorithms and connecting physical parameters with geometry of the problem under study. For computational grid construction, the standard OpenFOAM utilities, such as 'blockMesh', 'topoSet', and 'refineMesh', were used, as well. The main OpenFOAM C++ class 'polyMesh', which handles a grid, is constructed using the minimum amount of information necessary to determine the partition elements and parameters such as vertices, edges, faces, cells, blocks, external boundaries, etc. By choosing an appropriate type of computational grid, i.e. structured or unstructured, orthogonal or non-orthogonal, consistent with boundaries of a domain or inconsistent ones, each of which normally has its own advantages and disadvantages, one can provide successful searching for solution of a problem under study. Therefore, methods for grid construction were chosen individually for a particular problem based on values of typical length scales and geometric complexity of a problem under consideration [13].

An unstructured grid, which consists usually of 2D triangles or 3D tetrahedrons, can be applied to domains with arbitrary geometry without any restrictions on form and number of boundaries of a computational domain. Due to a high level of automation, it is possible to reduce significantly duration of grid reconstruction. However, the main disadvantage of such a grid is an irregular structure of data, which requires sophisticated methods for numerical solution of problems. Numerical algorithms are complicated, as well, by usage of unstructured grids, requiring additional memory to store data on connections between grid cells. Furthermore, increase in number of tetrahedral cells, compared to that of hexahedral type, imposes more requirements for operational memory resources.

Structured grids matching the external boundaries of a computational domain are believed to be the most effective ones, which enable implementing computational algorithms with a higher order accuracy and reducing both computation time and

amount of RAM required. By creating a curvilinear mesh, one can align grid lines with boundaries of a domain and, thereby, simplify specification of boundary conditions. However, a number of additional terms usually appear in governing equations due to a corresponding coordinate transformation. At the same time, procedures of a regular grid construction require a certain level of skills, efforts and computing resources, and can be applied only to a rather simple geometry of computational domain.

If it is impossible to construct a single mesh for a whole computational domain, grid is divided into a certain number of blocks. Complexity of such an approach consists in need for implementation of merging the solutions obtained in different subdomains. However, the technique for construction of a block-structured computational grid provides wide opportunities for using efficient numerical methods inside individual blocks with a regular grid structure.

Computation domain for the problems under consideration is a rectangle, which is divided into seven blocks. An obstacle is located in the central part of the computation domain, which is a plate or a horizontal wedge with length, $L = 10$ cm, and thickness, $h = 0.5$ cm, or height of the base, $h = 2$ cm, respectively (Fig. 2).

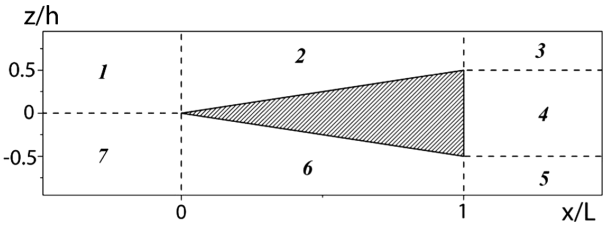

Fig. 2. Scheme of the computational domain partitioning into blocks.

The procedure for spatial discretization of the problem is parameterized that enables reducing significantly duration of grid reconstruction when changing parameters of the problem. The geometry of the computational domain allows constructing a block-structured hexahedral computational grid with nodes aligned at the block interfaces. Test computations with different grid resolutions confirm the need for resolving the smallest micro-scales of the problems, since a relatively coarse grid with total number of cells, $N_c = 5 \cdot 10^5$, gives unstable solution. Thus, numerical simulation of even 2D problems on continuously stratified fluids flows around impermeable obstacles require high-performance computing.

Algorithm for discretization of the computational domain involves mesh grading towards the obstacle (Fig. 3a). Near the body, the aspect ratio of a grid cell is approximately equal to unity, which has a positive effect on convergence of the solution. The main disadvantage of this method consists in necessity of cells rearrangement in all the subdomains at once if a grid is reconstructed, which leads to significant increase in computation time. In order to improve the quality of the computational domain discretization the OpenFOAM utilities, such as 'topoSet' and 'refineMesh', are additionally used, which enable selecting computational subdomains of interest and locally refining

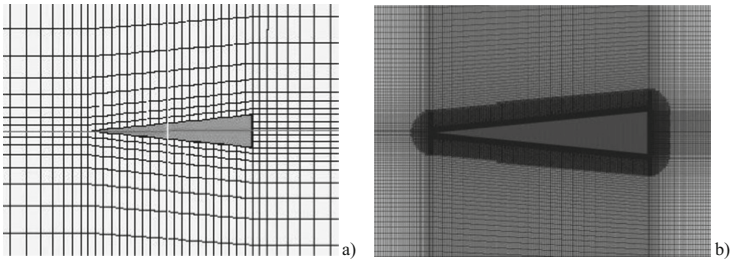

Fig. 3. The scheme of the computational domain partitioning: (a) – with a linear grid refinement, (b) – with an additional local partition.

them in accordance with prescribed scales and selected directions (Fig. 3b). The minimum mesh size of $2.5 \cdot 10^{-3}$ cm near impermeable boundaries satisfactorily resolves the diffusion microscale $\delta_N^{\kappa_S}$ with a relatively small total number of grid cells of 10^6 order.

However, partitioning of the grid cells even in a small part of the calculation domain requires a corresponding decrease in time step that, in turn, leads to an increase in duration of the computations. An essential disadvantage of additional local partitioning is a significant change in size of the grid cells on the boundary of subdomains that can affect the calculation results. By checking the constructed computational grid with the utility 'checkMesh' we make sure of its compliance with a set of constraints associated with the topology of the external boundaries and geometric characteristics of the grid cells, i.e. aspect ratio, skewness, twisting, non-orthogonality, etc.

Discretization of the boundary conditions (2) was carried out using the standard and extended utilities of the OpenFOAM package. The boundary condition on the surface of an obstacle for salinity perturbation gradient, which depends on orientation of the normal unit vector to the surface, was implemented by forming a non-uniform list of the field values using the standard, extended and self-elaborated utilities of the package. 'Empty' boundary conditions were set on the front and back faces of the computational domain, which exclude computations of the 2D problem in the third dimension.

To solve the resulting system of linear equations different iterative methods were used such as conjugate gradient method with PCG preconditioning applied to symmetric matrices and biconjugate gradient method with PBiCG preconditioning used for asymmetric matrices. As preconditioners for symmetric and asymmetric matrices DIC and DILU procedures were chosen, which are based on simplified procedures of incomplete Cholesky and LU factorization respectively. For coupling equations for momentum and mass conservation a steady well-convergent algorithm PISO (Pressure-Implicit Split-Operator) was used, which works in the most effective way for transient problems.

The need for a high spatial resolution of the problem results in a quite large number of computational cells that makes it irrational performing computations on a single-processor computer. Decomposition of the computational domain for a parallel run is carried out by a simple geometric decomposition in which the domain is split into pieces in certain directions with an equal number of computational cells in each block.

Such an approach allows setting a high spatial resolution of the computational domain and studying the problem in a wide range of the basic parameters for a quite reasonable time. The computations were performed in parallel using computing resources of the supercomputer "Lomonosov" of the Scientific Research Supercomputer Complex of MSU (SRCC MSU) and the technological platform UniHUB, which provides direct access to the Joint Supercomputer Center Cluster of the RAS (JSCC RAS).

The calculations were terminated when the integral characteristics or their statistical evaluations took values of steady-state regime. The spatial dimensions of the computational cells were chosen from the condition of adequate resolution of the fine flow components associated with the stratification and diffusion effects, which impose significant restrictions on the minimum spatial step. In high-gradient regions of the flow, at least several computational cells must fit the minimal linear scale of the problem. Calculation time step, Δt, is defined by the Courant's condition, $\mathrm{Co} = |\mathbf{v}|\Delta t/\Delta r \leq 1$, where Δr is the minimal size of grid cells and $\mathbf{v}$ is the local flow velocity. Additional control was ensured by comparison of independent calculations for fluids with different stratification.

5 Calculation Results

5.1 The Structure of Diffusion-Induced Flow on a Motionless Plate

In contrast to the stationary solutions by Prandtl [14], which lose regularity on horizontal surface, the complete solution of the Eq. (1) for transient flow remains finite for any sloping angle of the surface. A cellular flow structure is kept in patterns of all the physical variables, but thicknesses of interfaces are specific for each parameter.

The calculated pattern of diffusion-induced flow on the horizontal plate, which simulates the central section of impermeable obstacle with an arbitrary shape (Fig. 4a), consists of a layered sequence of symmetrically arranged horizontal vortex cells [13].

Fig. 4. The diffusion-induced flows on an obstacle with horizontal boundaries: (a) – calculated pattern of streamlines around the plate; (b, c) – patterns of density gradient field around the horizontal disc, calculated numerically and schlieren-visualized in a laboratory tank.

Uniformity of the streamline pattern indicates similarity of the velocity profile along the most length of the plate except for the narrow transition regions around its edges. Values of fluid velocity and vorticity decrease sharply with distance from the plate surface.

Even a small deviation from the horizontal position of the plate leads to violation of the flow symmetry and formation of new circulation systems including ascending and

descending jets along the upper and lower sides of the plate respectively, and a system of compensating circulating cells, as well [13]. The calculated and observed patterns of the density gradient fields on the plate and disc are in a good agreement (Fig. 4b and c).

5.2 Diffusion-Induced Flow on a Wedge

An impermeable obstacle immersed in a stably stratified fluid at rest forms a complex system of flows including the main thin jets along the sloping sides of the obstacle with the adjacent compensating counterflows [15]. With a distance from the obstacles, the layered structures are enlarged and the maximum fluid velocity decreases. Pattern of the horizontal component of salinity gradient shows a multiscale flow structure, including extended side flows and wavy structures (Fig. 5).

Positive values of a visualized field are coloured green, while negative ones are in blue. Differences in values of a field between neighboring isolines are the same. The side boundaries of a wedge-shaped obstacle with length, L = 10 cm, and maximal thickness, h = 2 cm, can be either straight or curved in form of a concave or convex arc [16].

The additional fine-structure flow components, such as dissipative-gravitational waves, are formed in form of rosettes around the corner points of the wedge, where maximum value of the longitudinal component of salinity gradient, $|\partial s/\partial x|_{\max} = 4 \cdot 10^{-2}$, is observed, while the corresponding value of salinity perturbation s is an order of 10^{-5}.

Structure of the horizontal component of salinity gradient field depends essentially on sign of the curvature of the wedge surface, the sharper the edges of the wedge the more pronounced the visualized beams of strips with alternating signs (Fig. 5a). At the same time, the maximum values are weakly dependent on curvature of the wedge sides. For a convex wedge (Fig. 5b) when angle between the base and the side edge is close to 90° the beam of fine structure elements is widened.

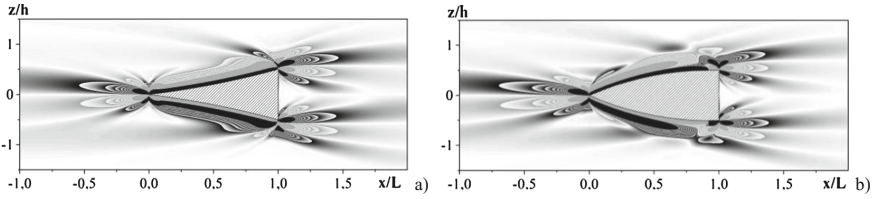

Fig. 5. Field of the longitudinal component of salinity gradient, $\partial s/\partial x$, around a wedge with concave (a) and convex (b) side boundaries (L = 10 cm, h = 2 cm, $T_b = 6.28$ s, $\tau = t/T_b = 16$)

In the pattern of pressure perturbation field there is a deficit pronounced in front of the tip, manifestation and height of which depends on curvature of the wedge side (Fig. 6). This deficit zone causes pressure difference which results in self-motion of a free wedge with neutral buoyancy observe in laboratory experiments.

The initial structure of the medium formed by diffusion-induced flows is changed dramatically with start of forced motion of a body even with the lowest velocity

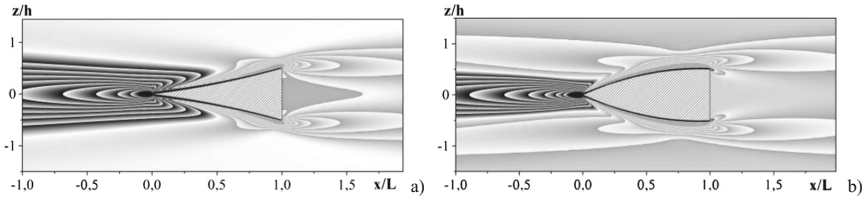

Fig. 6. Fields of pressure perturbation, P, around a wedge with concave (a) and convex (b) side boundaries (L = 10 cm, h = 2 cm, $T_b = 6.28$ s, $\tau = t/T_b = /16$ τ = 16).

comparable with the typical velocities of the diffusion-induced flow (Fig. 7). Upstream perturbations, rosettes of transient and extended fields of attached internal waves and downstream wake past extreme points of the body are formed in a continuously stratified fluid. Number of the attached internal waves observed, which do not penetrate into the wake behind the body, increases with time.

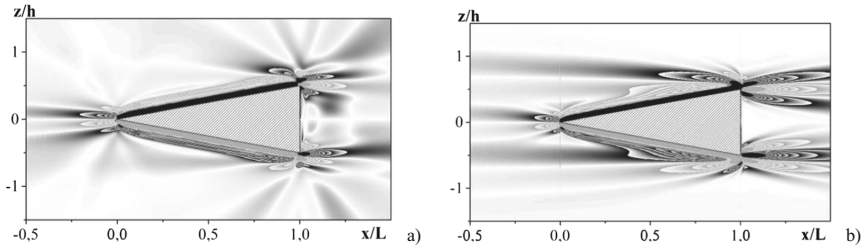

Fig. 7. Evolution of the horizontal component of salinity gradient perturbation field after start of motion of a wedge with straight boundaries (L = 10 cm, h = 2 cm, $T_b = 6.28$ s, U = 0.001 cm/s): (a, b) – $\tau = t/T_b = 2;\ 50$.

Structure of the calculated patterns of flow around a wedge is in an agreement with the schlieren visualization of refraction coefficient gradient field in a laboratory tank by "color shadow method" with a horizontal slit and grating for the bodies with other geometrical forms [11].

5.3 Flow Around a Rectangular Strip

The fundamental system of equations allows calculating a complete flow pattern and determining forces acting on a moving obstacle with a high degree of accuracy in a wide range of parameters without additional hypotheses and constants. This allows tracing a consistent restructuring of the flow due to "inclusion" of new components such as internal waves at start of motion, non-stationary vortices in the wake past an obstacle or rolling vortices along its surface (Fig. 8).

For all the velocities of the body motion, the flow field is characterized by a complicated internal structure. In the flow pattern around motionless body dissipative

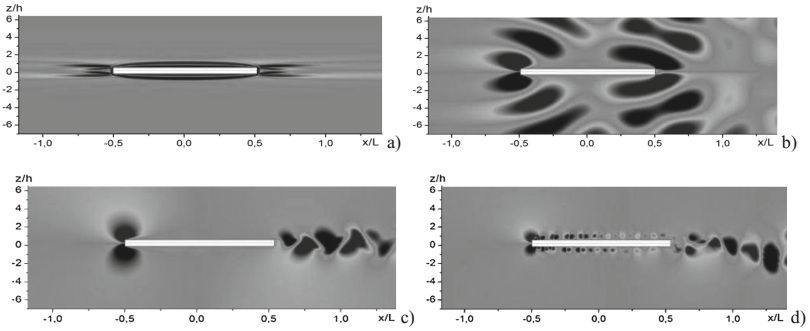

Fig. 8. Field of the vertical component of velocity around the plate ($N = 1.2\,\mathrm{s}^{-1}$, L = 10 cm, h = 0.5 cm): (a) – diffusion-induced flow for $U = 0$; (b–d) – $U = 1.0$; 5.0; 80 cm/s, $\mathrm{Re} = 10^3$; $5 \cdot 10^3$; $8 \cdot 10^4$, $\mathrm{Fr} = U/NL_x = 0.1$; 0.5; 6.7, $\lambda = UT_b = 5.2$; 26; 418 cm.

gravity waves are manifested at the edges of the strip (Fig. 8a). Around the slowly moving body a group of attached waves with lengths, $\lambda = UT_b = 5.2$ cm, are formed at the edges of the plate in opposite phases (Fig. 8b). Then, the main flow components become vortices, which are formed around the leading edge of the plate and manifested downstream in the wake (Fig. 8c). With further increase in velocity of the body motion, the flow pattern becomes more and more non-stationary (Fig. 8d).

Patterns of other fields have even more complicated fine structure. For comparison, Fig. 9 shows patterns of pressure and density gradients fields, as well as baroclinic vorticity generation and mechanical energy dissipation rates for both the strongly stratified and potentially homogeneous fluids.

Complexity of the patterns of the pressure and density gradients fields shown in Fig. 9 is attributable to the properties of differential operators generating two groups of spots for each vortex core, which correspond to the regions of perturbation growth and attenuation respectively. At the same time, advantage of studying these patterns consists in a more complete visualization of the structural details, which makes it possible to identify small-scale elements against the background of larger ones.

The transverse dimensions of the flow components, which are determined by the values of kinetic coefficients in the given mathematical formulation, are minimal in the patterns of the density gradient fields. The pressure gradient fields are generally smooth, but close to the leading edge there are large variations due to the simultaneity of generation of the both large (internal waves, vortices) and fine flow components (Fig. 9a, b).

In the pattern of the horizontal component of pressure gradient, $\partial P/\partial x$, (Fig. 9a) a sequence of spots with different signs is manifested like in the vertical component of velocity field in Fig. 8d. At the time distribution of the vertical component of pressure gradient, $\partial P/\partial z$, shown in Fig. 9b, demonstrates a more rarefied set of vertically oriented spots with different colours. Here, the vortices are well resolved and, in particular, there are ten cores above the plate, as it is seen from the patterns in Fig. 9, which is greater by one compared that to the case of the horizontal component of velocity field.

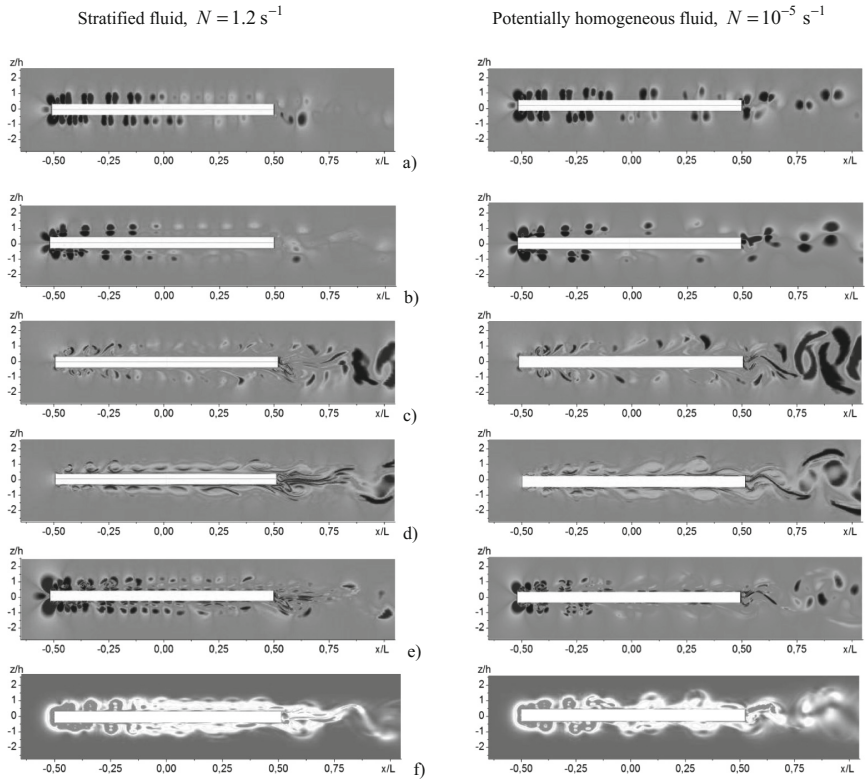

Fig. 9. Calculated patterns of instantaneous fields near the plate (L = 10 cm, h = 0.5 cm, U = 80 cm/s) in the stratified (left column $N = 1.2\,s^{-1}$, Fr = 6.7) and potentially homogeneous fluids (right column $N = 10^{-5}\,s^{-1}$, Fr = $8 \cdot 10^5$): (a, b) – horizontal and vertical components of pressure gradient, (c, d) – horizontal and vertical components of density gradient, (e) – baroclinic vorticity generation rate, (f) – mechanical energy dissipation rate.

Even a more complicate flow pattern is resolved near the leading edge. In the weakly stratified fluid, the perturbations degenerate more slowly as compared to that in the strongly stratified medium and scales of the vortex structures are noticeably smaller.

The patterns of the components of density gradient are presented in Fig. 9c, d. In the horizontal component of the density gradient field, thin layers with the both signs are localized on the vortex shells, which are combined into compact spots behind the body. In the weakly stratified fluid, the structures of the vertical component of density gradient are oriented mostly horizontally and form its own system of spiral curls typical for vortex elements. The local patterns of the physical variables in Fig. 9c, d are substantially different, locations of the centers of the regions, which they outline, not coinciding.

It should be specially noted, the differences in the geometry and fine structure of the pressure and density gradients fields, which determine the spatial and temporal variations of such a dynamic parameter as vorticity generation rate of the flow and, hence, change in value of the vorticity itself.

Due to the differences in the spatial and temporal scales of the flow components, a general inhomogeneous distribution of the forces acting on the body, i.e. compression on the leading edge and stretch at the initial section of the side surface, is here supplemented with large variations in space and time. Further in the pressure field, deficit zones (side stretching) are expressed due to the passage of centers of large vortices, which are the main sources of the side surface oscillation leading to development of such dangerous phenomena as buffeting and flutter. The difference in the fine details of the pressure gradient fields in the wake of the body is due to the effects of buoyancy forces, suppressing fluid transfer in the vertical direction, and the fine flow components.

There are two particular flow regions located exactly near the leading and trailing edges of the plate, where the main generation of vorticity vector, $\mathbf{\Omega} = \mathrm{rot}\ \mathbf{v}$, occurs as a consequence of both the overall reorganization of the velocity field and the baroclinic effects. Geometry of the density gradients field is complicated as the layered flow structure is developed downstream from the leading edge. In the weakly stratified fluid, range of oscillations of the vortices' size in the wake increases with distance from the trailing edge when stabilizing buoyancy forces are absent.

Pattern of the streamwise component of the baroclinic vorticity generation rate, $d\mathbf{\Omega}/dt = \nabla P \times \nabla(1/\rho)$, is presented in Fig. 9e, which is determined by the non-collinearity of pressure ∇P and density gradients $\nabla\rho$ according to the Bjerknes theorem. This field is the most complex and structured one in flows of inhomogeneous fluids. There are regions of its generation and dissipation with size of an order of the plate's thickness manifested above and below the leading edge and in front of the body respectively. Further downstream, the structures get thinner, and in addition to the remaining vortex elements a number of multiple thin zones of vorticity amplification and decay appear, which are gradually lengthened.

Fine linear structures are predominantly manifested in the wake behind the trailing edge of the plate, which are oriented mainly in the direction of the flow and deformed by the large irregularities. In the strongly stratified fluid, the perturbations of the both signs are expressed along the whole length of the plate, but in the potentially homogeneous one they are only in the first quarter. There are regions of vorticity generation and dissipation manifested in the areas of interaction of the vortices with the free stream in the wake of the body. The geometry of the baroclinic vorticity generation rate field explains the formation dynamics of vortex flow fine structure and the mechanism for splitting of the fields into a set of layered structures observed in the schlieren images of the wake flows [10, 11].

Field of the mechanical energy dissipation rate, $\varepsilon = 0.5\rho\nu(\partial v_i/\partial x_k + \partial v_k/\partial x_i)^2$, presented in Fig. 9f, is different from zero in a relatively narrow zone in front of the body, where the horizontal flow turns flowing the plate, and reaches maximal values in the vortex structures at the first third of the plate's length. Regions of dissipation, observed at the second half of the plate, are larger in the potentially homogeneous fluid, compared to that for the strongly stratified one. It should be noted a qualitative difference in geometry of the vorticity generation rate field with its pronounced fine structures (Fig. 9c) and a relatively smooth distribution of the energy dissipation rate field (Fig. 9f).

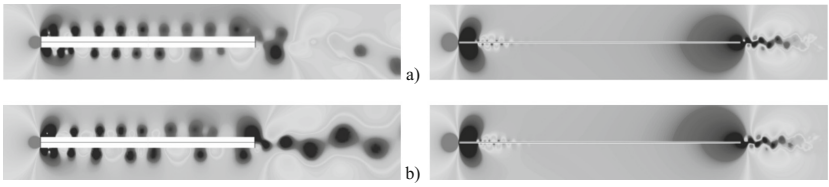

Fig. 10. Patterns of the pressure field around the horizontal plate (L = 10 cm, h = 0.5 cm, U = 80 cm/s): thick (h = 0.5 cm, left) and thin (h = 0.05 cm, right) ones: (a, b) – $N = 1.2\,s^{-1}$ and $N = 0$.

All the instantaneous flow patterns including the vorticity generation fields in Fig. 9 are in a continuous evolution. The variation of the velocity pattern in the kinematic description is caused by the generation and break-up of new elements, such as vortices due to the non-synchronized variation of the physical parameters with thermodynamic nature, in particular, density and pressure gradients.

In the dynamic description, the generation of new elements with their own kinematics and spatial and temporal scales is associated with the high order and nonlinearity of the fundamental system of equations. Even in the linear approximation, the complete solutions of this system contain several functions, which can be treated in the nonlinear models as analogues of the components interacting with each other and generating new types of disturbances [7].

The pressure perturbation field shows a strong dependence on the vertical dimension of the obstacle. In the wake past the thick plate, a number of large vortices develop (Fig. 10, left column), while past the thin plate the transverse streaky structures are manifested similar to ones observed in the experiments (Fig. 1). A more complete collection of flow patterns past the plates with different shapes are presented in [8, 17].

6 Conclusion

Based on the open source software 2D numerical simulations of incompressible stratified (strongly and weakly) and homogeneous (potentially and actually) fluids flows were performed. The method allows analyzing in a single formulation the dynamics and fine structure of flow patterns past obstacles in a wide range of stratification and flow parameters.

Transient flow patterns past obstacles were analyzed, and physical mechanisms were determined, which are responsible for formation of vortices in regions with high pressure and density gradients near the edges of an obstacle. The calculation results are in a qualitative agreement with the data from laboratory experiments.

Flow around obstacles is a complex, multiscale, and transient physical process, which requires additional detailed experimental and theoretical study accounting for the effects of diffusion, thermal conductivity, and compressibility of the medium with control of the observability and solvability criteria for all the physical parameters and structural components of the flows under study.

Acknowledgements. The work was partially supported by Russian Foundation for Basic Research (grant 15-01-09235). The calculations were performed using the service UniHUB (www.unihub.ru) and Research Computing Centre "Lomonosov" (www.parallel.ru).

References

1. D'Alembert, J.-R.: Traitè de l'èquilibre et de movement des fluids. Paris, David. 458 p. (1744)
2. D'Alembert J.-R.: Réflexions sur la cause générale des vents. Paris (1747)
3. Euler, L., Robins, B.: Neue Grundsätze der Artillerie enthaltend die Bestimmung der Gewalt des Pulvers nebst einer Untersuchung über den Unterscheid des Wiederstands der Luft in schnellen und langsamen Bewegungen. Aus d. Engl. übers. u. mit Anm. v. L. Euler. Berlin, Haude, 720 S. (1745)
4. Euler, L.: Principes généraux du mouvement des fluids. Mémoires de l'Academié royalle des sciences et belles letters. Berlin. vol. 11 (papers of 1755 year). (1757)
5. Landau, L.D., Lifshitz, E.M.: Fluid Mechanics: Course of Theoretical Physics, vol. 6, p. 731. Pergamon Press, Oxford (1987)
6. Baidulov, V.G., Chashechkin, Y.: Invariant properties of systems of equations of the mechanics of inhomogeneous fluids. J. Appl. Math. Mech. **75**(4), 390–397 (2011). http://www.sciencedirect.com/science/journal/00218928
7. Chashechkin, Y.D.: Differential fluid mechanics – harmonization of analytical, numerical and laboratory models of flows. In: Neittaanmäki, P., Repin, S., Tuovinen, T. (eds.) Mathematical Modeling and Optimization of Complex Structures. CMAS, vol. 40, pp. 61–91. Springer, Heidelberg (2016). doi:10.1007/978-3-319-23564-6_5
8. Zagumennyi, Y.V., Chashechkin, Y.D.: Pattern of unsteady vortex flow around plate under a zero angle of attack. Fluid Dyn. **51**(3), 53–70 (2016). doi:10.7868/S056852811603018X
9. Schlichting, H.: Boundary-Layer Theory, p. 535. McGraw-Hill, New York (1955)
10. Bardakov, R.N., Mitkin, V.V., Chashechkin, Y.: Fine structure of a stratified flow near a flat-plate surface. J. Appl. Mech. Technol. Phys. **48**(6), 840–851 (2007). doi:10.1007/s10808-007-0108-6
11. Chashechkin, Y.D.: Structure and dynamics of flows in the environment: theoretical and laboratory modeling. In: Actual Problems of Mechanics. 50 years of the A.Y. Ishlinskiy Institute for Problems in Mechanics of the RAS, pp. 63–78. (2015) (in Russian)
12. Dimitrieva, N.F., Zagumennyi, Y.V.: Numerical simulation of stratified flows using OpenFOAM package. In: Proceedings of the Institute for System Programming RAS, vol. 26, no. 5, pp. 187–200 (2014). doi:10.15514/ISPRAS-2014-26(5)-10
13. Zagumennyi, I.V., Chashechkin, Y.D.: Diffusion-induced flow on a strip: theoretical, numerical and laboratory modeling. Procedia IUTAM. **8**, 256–266 (2013). doi:10.1016/j.piutam.2013.04.032
14. Prandtl, L.: Führer durch die Strömungslehre. Braunschweig: Vieweg. 638 p. (1942)
15. Dimitrieva, N.F., Chashechkin, Y.: Numerical simulation of the dynamics and structure of a diffusion-driven flow on a wedge. Comput. Contin. Mech. **8**(1), 102–110 (2015). doi:10.7242/1999-6691/2015.8.1.9
16. Zagumennyi, Ia.V., Dimitrieva, N.F.: Diffusion-induced flow on a wedge-shaped obstacle. Phys. Scr. **91**, Article No.084002 (2016). doi:10.1088/0031-8949/91/8/084002
17. Chashechkin, Y.D., Zagumennyi, I.V.: Hydrodynamics of horizontal stripe. Probl. Evol. Open Syst. **2**(18), 25–50 (2015). (The Republic of Kazakhstan)